

SU(4)-symmetric Hubbard model at quarter filling: insights from the dynamical mean-field approach

Vladyslav Unukovych¹ and Andrii Sotnikov^{1,2,*}

¹Karazin Kharkiv National University, Svobody Sq. 4, 61022 Kharkiv, Ukraine

²Akhiezer Institute for Theoretical Physics, NSC KIPT, Akademichna Str. 1, 61108 Kharkiv, Ukraine

(Dated: June 26, 2022)

We apply dynamical mean-field approach to the four-component SU(4)-symmetric Fermi-Hubbard model to study transitions between different magnetically-ordered phases as well as hysteresis behavior in the unordered regime. At quarter filling (one particle per site) we identify both the two-sublattice and plaquette-ordered antiferromagnetic phases with the corresponding entropy-driven hierarchy for critical temperatures. We also analyze the behavior of thermodynamic characteristics: the local double occupancy, compressibility, and entropy per particle, which are relevant for experiments with ultracold alkaline-earth(-like) atoms in optical lattices.

I. INTRODUCTION

Ultracold atomic gases in spatially-periodic potentials serve as a good platform for the detailed exploration of conventional systems, such as the multi-orbital Hubbard model, as well as of exotic states of matter with high symmetries. In particular, with ultracold ytterbium-173 and strontium-87 atoms one can realize high-symmetry groups, such as SU(N) with the number N as high as $N = 6$ and $N = 10$, respectively [1–3]. The central object of the current study — the four-component quantum system with an SU(4) symmetry — can be acquired with these atomic species by removing exceeding number of components with certain nuclear spin projections. The remaining four internal states of an atom can be viewed then as distinct flavors or *pseudospin components*.

By now, the theoretical studies of the SU(4)-symmetric Hubbard model with respect to optical-lattice realizations were mostly focused on the case of the half-filled lowest band, see, e.g., Refs. [4–8]. In contrast, due to complexity of the respective theoretical analysis (in particular, due to the sign problem in the corresponding quantum Monte Carlo simulations), the case of average filling by one particle per site is much less explored [9], despite its significance. For instance, in the limit of large local interaction and one particle per site the SU(4)-symmetric Hubbard model can be transformed into the corresponding Heisenberg model, which has been investigated by a number of advanced theoretical approaches by now, see, e.g., Refs. [10–12]. According to some of them, in the zero-temperature limit a specific Néel-type arrangement of atoms can develop on the square lattice, which we call below as *plaquette order*. At the same time, by accounting for thermal excitations, i.e., with the entropy increase it is argued that the system can undergo a transition to the antiferromagnetic state with a conventional bipartite structure [12].

From the experimental perspective, the low-temperature regimes in the gases of alkaline-earth(-like)

atoms (AEAs), e.g., ⁸⁷Sr or ¹⁷³Yb, are believed to become more accessible due to recent advances in cooling techniques [13, 14] and quantum gas microscopy [15, 16]. This raises important questions on whether the many-body phases peculiar to the SU(4)-symmetric Heisenberg model remain stable under inclusion of hopping processes and thermal excitations. Moreover, for practical purposes not only qualitative, but quantitative estimates and the choice of optimal physical parameters are needed to approach particular many-body regimes.

In this paper, we study how the correlations between pseudospin components, which are peculiar to the Heisenberg model, evolve by transforming to the more generic Hubbard model with an SU(4) symmetry. We determine stability of certain many-body regimes with respect to the change of the local interaction strength and temperature. Furthermore, we analyze important physical observables, which can serve as indicators of the onset of magnetic correlations and many-body phenomena in SU(4)-symmetric four-component Fermi gases in optical lattices.

II. MODEL AND METHOD

We describe the four-component interacting Fermi gas in the framework of the Hubbard model with four internal pseudospin states and the lowest-band approximation, which corresponds to the situation, where the effective band gap is much larger than the relevant energy scales (e.g., the noninteracting bandwidth and the interaction amplitude). This is realized by sufficiently strong lattice potential in all spatial directions, $V_{\text{lat}}^{(\alpha)} > 5E_r$, where $\alpha = \{x, y, z\}$ and $E_r = \hbar^2 k^2 / 2m$ is the recoil energy of an atom with the mass m in the optical lattice characterized by the wave number k . Below, we focus on the cases, where the motional degrees of freedom in one spatial direction are suppressed, while in the remaining two are equal, i.e., the atoms are loaded into the quasi two-dimensional square lattice potential. Furthermore, we make an assumption that the on-site interaction U can be set equal for all four components, which is valid

* a.sotnikov@kipt.kharkov.ua

for the ground-state manifold of AEAs, thus yields the Hamiltonian

$$\hat{\mathcal{H}} = -t \sum_{\langle i,j \rangle} \sum_{\alpha=1}^4 (\hat{c}_{i\alpha}^\dagger \hat{c}_{j\alpha} + \text{H.c.}) - \mu \sum_j \sum_{\alpha=1}^4 \hat{n}_{j\alpha} + U \sum_j \sum_{\alpha=1}^4 \sum_{\alpha' > \alpha} \hat{n}_{j\alpha} \hat{n}_{j\alpha'}, \quad (1)$$

where $\hat{c}_{i\alpha}^\dagger$ ($\hat{c}_{i\alpha}$) is the fermionic creation (annihilation) operator for a particle with flavor α located on lattice site i and $\hat{n}_{i\alpha} = \hat{c}_{i\alpha}^\dagger \hat{c}_{i\alpha}$ is the corresponding number operator. The hopping amplitude t and chemical potential μ are equal for all flavors and lattice sites. It is worth noticing that in the given form the Hamiltonian (1) is SU(4) symmetric.

The symmetry of the model can be better understood by employing the Schrieffer-Wolff transformation in the limit $t \ll U$ close to 1/4 band filling, $\sum_{\alpha} n_{i\alpha} \approx 1$, where one can map the Hamiltonian (1) to an effective one with the same symmetry, i.e., the SU(4)-symmetric Heisenberg model

$$\hat{\mathcal{H}}_{\text{eff}} = J \sum_{\langle i,j \rangle} \sum_{k=1}^{15} \hat{S}_{ki} \hat{S}_{kj} \quad (2)$$

with positive (antiferromagnetic) exchange coupling $J = 4t^2/U$. Here \hat{S}_k is the generator of the SU(4) symmetry group, i.e., the pseudospin projection operator to the k -th axis in the effective 15-dimensional spin space. It can be expressed through the generalized 4×4 Gell-Mann matrices $\lambda_k = \{\lambda_1, \dots, \lambda_{15}\}$ obeying standard commutation relations [17] similarly to the spin-1/2 case, $\hat{S}_k = \frac{1}{2} \hat{c}_{i\alpha}^\dagger \lambda_{k\alpha\beta} \hat{c}_{i\beta}$. Therefore, the introduced pseudospin operators \hat{S}_k can be viewed as the generators of the SU(4) group, since the operator

$$\hat{\mathcal{U}}(\varphi) = \exp \left(i \sum_{k=1}^{15} \varphi_k \hat{S}_k \right) \quad (3)$$

performs special ($\det \mathcal{U} = 1$) unitary rotations in the corresponding space (φ_k are arbitrary real numbers). Now, it can be directly verified that the original Hamiltonian (1) is invariant under these transformations in the introduced pseudospin space, $\hat{\mathcal{H}} = \hat{\mathcal{U}}(\varphi) \hat{\mathcal{H}} \hat{\mathcal{U}}^\dagger(\varphi)$.

To study thermodynamic properties and magnetic ordering phenomena, we employ the dynamical mean-field theory (DMFT) and its real-space generalization with clustering procedure [18–21]. Although DMFT is an approximate method for realistic lattice geometries, results obtained by this approach are valuable both for experiments and for more advanced methods, such as quantum Monte Carlo simulations, which are computationally rather demanding due to the generic presence of a sign problem for the Fermi-Hubbard model away from half filling.

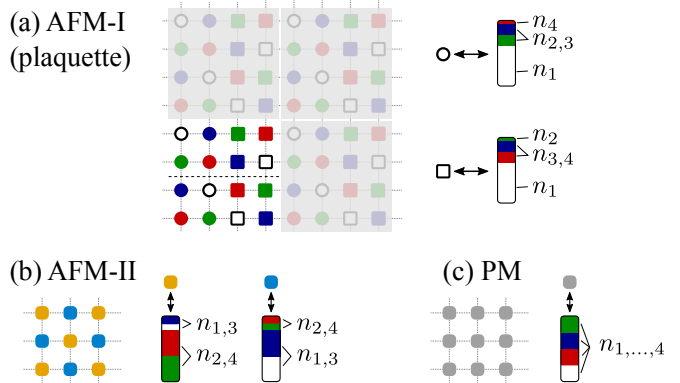


FIG. 1. Spatial configurations of local occupancies on square lattice: (a) plaquette-ordered state (the shaded regions are the same patterns that can be generated by regular lattice translations), (b) two-sublattice AFM, and (c) unordered paramagnetic (PM) state. The length of the color bars corresponds to $n = 1$, while their relative filling by different colors indicates the fraction n_{α} of the pseudospin components on the lattice site.

To solve the Anderson impurity problem in DMFT, we employ the exact-diagonalization (ED) procedure [22], since it is relatively fast and reliable in most regimes of interest for Fermi gases with four interacting flavors and the number of bath orbitals $n_s = 4$ per each component [8, 23]. To obtain the lattice Green's functions G_{σ} for self-consistency conditions in DMFT, one can express it in terms of the noninteracting density of states for a particular lattice geometry and the local self-energies Σ_{σ} calculated within the impurity solver. However, this approach works well only in the homogeneous or the bipartite-ordered, i.e., two-sublattice antiferromagnetic (AFM) regimes. In more general situation, e.g., the plaquette-ordered AFM state, see Fig. 1(a), we employ the real-space generalization with clustering procedure as, e.g., described in Ref. [21]. Within the latter approach, the corresponding lattice Green's function is obtained from the inversion of the following real-space matrix:

$$[\mathbf{G}_{\sigma}^{-1}(i\omega_n)]_{ss'} = [i\omega_n + \mu - \Sigma_{\sigma s}(i\omega_n)]\delta_{ss'} - t_{ss'}, \quad (4)$$

where the indices s, s' denote the lattice sites, $\delta_{ss'}$ is the Kronecker symbol, $\omega_n = \pi(2n + 1)/\beta$ is the fermionic Matsubara frequency, and β is the inverse temperature ($\beta = 1/k_B T$). The hopping matrix element $t_{ss'}$ equals t if there is tunneling possible between the lattice sites s and s' and zero otherwise, which depends on the lattice geometry, system size, and the boundary conditions of the original model (1).

As soon as the DMFT convergence criteria are fulfilled, the set of local observables is evaluated on each lattice site. In case it is not specified otherwise, below we employ the units of the hopping amplitude t in all energy-related quantities.

III. RESULTS

A. Order parameters and phase diagram

In the numerical analysis of the Hubbard model at quarter filling we observe two types of AFM-ordered states: AFM-I and AFM-II, which are schematically illustrated in Figs. 1(a) and (b), respectively. The low-temperature AFM-I configuration can be viewed as a generalization of the Néel-type dimer order in the SU(4)-symmetric Heisenberg model [11]. Indeed, in the limit $U \rightarrow \infty$ the difference between configurations that deviate only by minority contributions (encoded by the shape of symbols in Fig. 1(a)) vanish. But, as soon as the fluctuations originating from the hopping processes become sizeable, the minority contributions form an additional modulation. To determine the flavor, which has the least minor contribution on the given site in the observed AFM-I phase, it is sufficient to determine the flavor that has dominant contributions on two out of four nearest-neighbor sites. Obviously, this additional modulation (encoded by the shape of symbols in Fig. 1(a)) originates from the Pauli blocking of fermions hopping on nearest-neighbor sites. Note that although three combinations of minority occupancies is possible, it is sufficient to have two types of the described modulations to cover the whole plaquette in the closed and consistent way.

In the first place, we have to determine the boundaries between above-mentioned AFM and PM phases. For this purpose we introduce two positive-valued order parameters, m_1 and m_2 , as linear combinations of local occupancies n_i ,

$$\begin{aligned} m_1 &= n_{1*} - n_{2*}, \\ m_2 &= n_{1*} + n_{2*} + n_{3*} - 3n_{4*}, \end{aligned} \quad (5)$$

where the asterisk means that the flavors are permuted to yield the descending order of the respective values, i.e., $n_{1*} \geq \dots \geq n_{4*}$.

At variable local interaction strength U and temperature T , we obtain dependencies similar to those shown in Fig. 2. The magnetization behavior indicates that the transition from the AFM-II to PM is continuous, i.e., of the second order. At the same time, the transition from the plaquette-ordered AFM-I to AFM-II is of the first order. The latter is also related to the fact that any particular flavor in the AFM-I configuration, see Fig. 1(a), cannot pair up with another one everywhere, where they have dominant contributions, to fill every second site in the checkerboard manner.

Furthermore, we construct the phase diagram shown in Fig. 3. It clearly points to the absence of the ordering mechanism at weak coupling $U/t \lesssim 10$, i.e., in the Fermi liquid regime, where the system remains SU(4) symmetric down to zero temperature. However, as soon as the system undergoes the metal-insulator transition (the shaded region in Fig. 3), the AFM correlations between localized moments become crucial. We note that

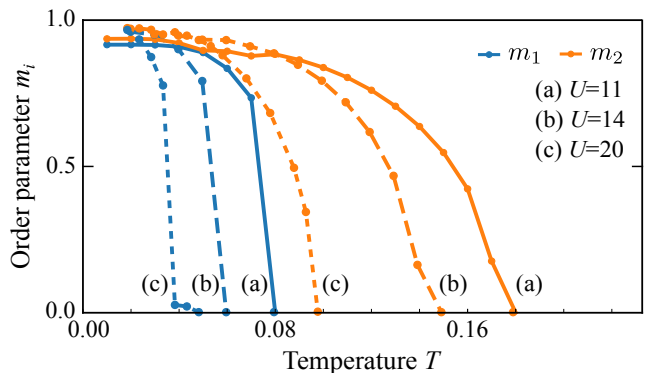


FIG. 2. Temperature dependencies of the local order parameters introduced in Eq. (5) at different interaction strengths U : (a) $U = 11$, (b) $U = 14$, and (c) $U = 20$.

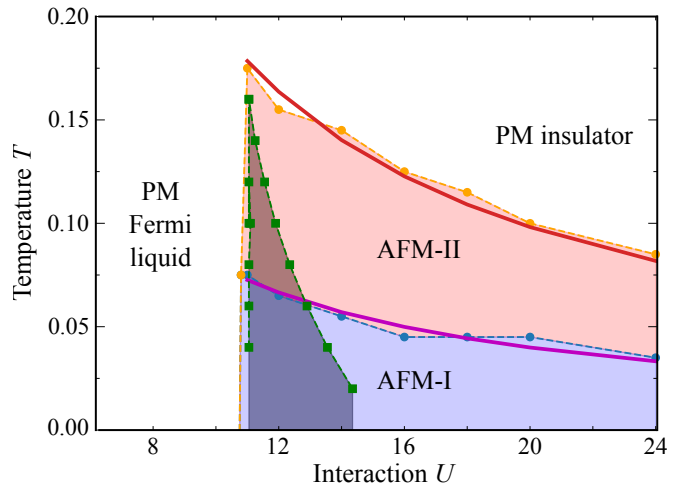


FIG. 3. Phase diagram of the SU(4)-symmetric Hubbard model at quarter filling. The symbols connected by thin lines correspond to DMFT data, while the thick solid lines are the least-square fits to the $T_c \propto t^2/U$ dependence, with the coefficients 0.79 and 1.96 for the lower and the upper phase boundary, respectively. The dark-shaded area is the metal-insulator hysteresis region obtained under the PM constraint.

there is an entropy-driven hierarchy of critical temperatures. Obviously, the AFM-II phase has a higher entropy capacity but cannot remain stable down to zero temperature due to the third law of thermodynamics. In contrast, in case the whole lattice can be covered by the finite-size plaquettes as in the AFM-I phase, see Fig. 1(a), this many-body configuration becomes consistent with the third law of thermodynamics. In this respect, one could also draw an analogy to the SU(3)-symmetric Hubbard model at $n = 1$ [21, 24].

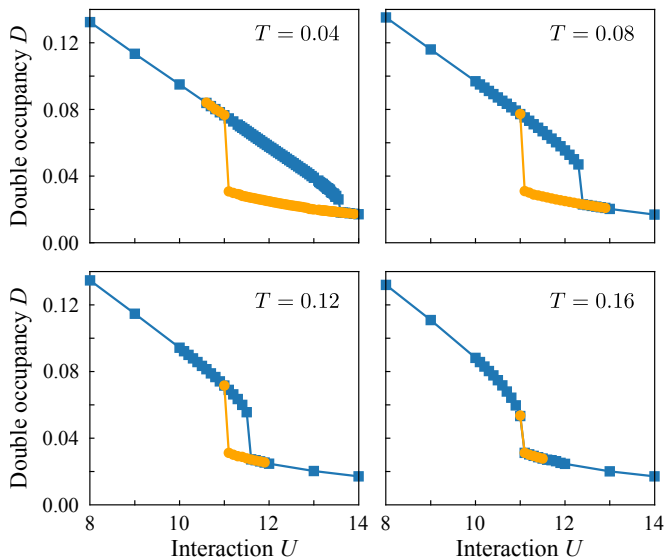


FIG. 4. Hysteresis behavior of the double occupancy as function of the interaction strength at constant temperature under the PM constraint in DMFT.

B. Metal-insulator transition and relevant observables

The employed theoretical approach allows us to analyze the behavior of local correlation functions. In particular, the double occupancy $D_j = \sum_{\alpha' > \alpha} \langle \hat{n}_{j\alpha} \hat{n}_{j\alpha'} \rangle$ is the one that can be effectively measured in cold-atom experiments [25]. Following the standard theoretical procedure, to exclude the impact of magnetic correlations, we artificially impose the translational symmetry on all lattice sites by the corresponding (paramagnetic) self-consistency conditions of DMFT. The observed behavior at constant temperature and continuous increase (decrease) of the interaction strength is shown in Fig. 4. The corresponding region with coexisting metallic and insulating solutions is also indicated in Fig. 3.

Note that one can typically suppress the magnetic correlations by introducing hopping process across one of diagonals, i.e., by a minor change of the lattice geometry towards the triangular one. In this way the hysteresis behavior in the paramagnetic regime can be more effectively decoupled from the onset of magnetic correlations.

The isothermal compressibility $\kappa_T = n^{-2}(\partial n / \partial \mu)_T$ is another accessible observable in cold-atom experiments. It can be measured through the variation of the trap curvature and subsequent analysis of the changes in the density profiles, see, e.g., Ref. [13]. In Fig. 5 we compare density distributions at four different interaction strengths and fixed temperature. These clearly indicate the formation of plateau structures in the Mott-insulating regime. According to Fig. 5, we also observe that the corresponding values of κ_T at $T = 0.1$ across the metal-insulator transition drop by around two orders of magnitude, e.g., $\kappa_T \approx 6 \times 10^{-2}$ and $\kappa_T \approx 4 \times 10^{-4}$ at $U = 10$ and $U = 12$,

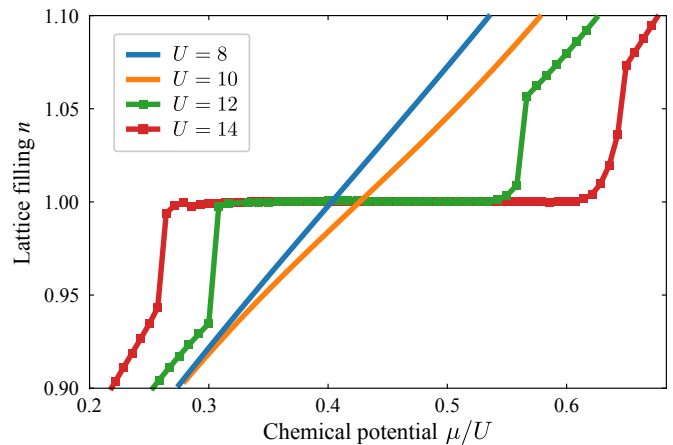


FIG. 5. Lattice filling as function of the chemical potential (in units of the respective interaction strength U) at $T = 0.1$ and different U . At $U = 12$ and $U = 14$ the plateau structures are accompanied by the AFM-II ordering.

respectively. By means of the local-density approximation the depicted dependencies can also be transformed to the spatial density distributions in the trap, e.g., $n(r)$ by taking $\mu(r) = \mu_0 - V_0 r^2$ in case of isotropic harmonic trapping potential with the amplitude V_0 .

C. Entropy analysis

Within access to the density distribution $n(\mu)$ of the interacting Fermi gas as a function of the chemical potential (see also Fig. 5), one can determine the entropy per particle s , which can be viewed as more relevant thermodynamic quantity (compared to the temperature T) in cold-atom experiments. To this end, we employ the Maxwell relation in the integral form, $s = \int_{-\infty}^{\mu_1} \left(\frac{\partial n}{\partial T} \right) d\mu$, where the upper limit μ_1 is determined from the condition $n(\mu_1) = 1$.

According to Fig. 6, in the region of weak and intermediate coupling, the well-known Pomeranchuk cooling effect is observed [25], i.e., at fixed entropy the temperature decreases with increasing interaction strength. For the SU(4)-symmetric Fermi gas at quarter filling, the critical entropy value at which the isentropic curve reaches the estimated peak of the AFM-II phase (see also Fig. 3) is $s_c^{\max} \approx 1.38 k_B$. This value significantly exceeds the corresponding critical value for AFM ordering in the SU(4)-symmetric Hubbard model at half filling ($n = 2$) [8] and the critical value for orbital ordering in the four-component SU(2) \times SU(2)-symmetric ytterbium-173 Fermi gas at $n = 1.5$ [26]. Therefore, according to typical experimental limitations in the entropy per particle, the observation of magnetic correlations in the SU(4)-symmetric Hubbard model at quarter filling looks advantageous.

Note that the calculated entropy values correspond to the bulk properties of the system. In fact (we also verified

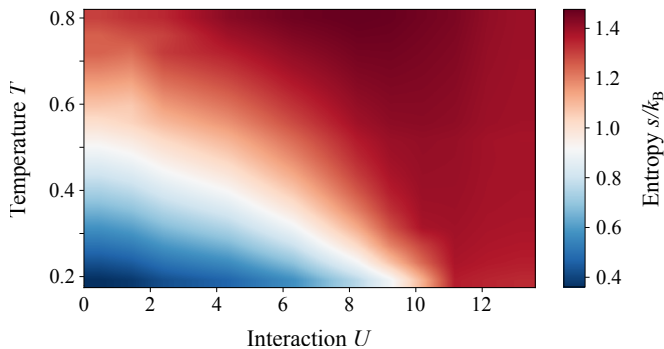


FIG. 6. Contour plot of the entropy per particle as a function of the temperature and interaction strength in the SU(4)-symmetric Hubbard model at $n = 1$.

that within a direct DMFT analysis), in the trapped system the metallic shells with $n < 1$ possess higher entropy per particle. This means that in case one realizes the inhomogeneous system with $n \approx 1$ in the central region to approach magnetic ordering, the estimated theoretical bounds for the total entropy per particle S_{tot}/N can be further increased.

IV. CONCLUSION

We studied low-temperature characteristics of four-component Fermi gases in optical lattices described by the SU(4)-symmetric Hubbard model at quarter filling. The model itself can govern not only the low-temperature behavior of cold-atom systems, but also certain classes of crystalline materials [27].

The theoretical analysis was developed in the framework of the dynamical mean-field theory. It is shown that in quasi-two-dimensional square lattice geometry the system undergoes the entropy-driven sequence of phase transitions as soon as the local interaction between atoms is sufficient for the onset of the insulating regime, i.e., at $U \gtrsim 11t$. The observed plaquette ordering in the system under study can be viewed as a generalization of the

limiting case – the Néel-ordered dimer configuration analyzed in the framework of the SU(4)-symmetric Heisenberg model [11]. At the same time, the studied two-sublattice AFM-II phase with the higher entropy capacity emerges similarly as in the SU(3)-symmetric Hubbard model [21] or as in SU($N \geq 3$)-symmetric Heisenberg models [12].

By means of DMFT we also analyzed the metal-insulator hysteresis region and identified that its temperature range practically coincides with the range for magnetic ordering, in contrast to the Hubbard model with two or three interacting components. Our entropy analysis suggests that this first-order metal-insulator phase transition region (in contrast to the high- T crossover regime) can be accessed in current and near-future experiments with the alkaline-earth-like atoms in optical lattices.

In addition to measuring magnetic correlations between different fermionic flavors or analyzing related structure factors, we suggested other related thermodynamic quantities as potential indicators of phase transitions and many-body phenomena in the system under study. In particular, the double occupancy and compressibility also show clear signals across the phase boundaries. The obtained entropy dependencies provide with quantitative information on how the system can be effectively cooled by means of the Pomeranchuk effect and whether the phases under study can be effectively approached starting from certain initial values of the gas temperature.

ACKNOWLEDGMENTS

The authors acknowledge support by the National Research Foundation of Ukraine, Grant No. 0120U104963 and the Ministry of Education and Science of Ukraine, Research Grant No. 0120U102252. Access to computing and storage facilities provided by the Poznan Supercomputing and Networking Center (EAGLE cluster) is greatly appreciated.

-
- [1] C. Wu, *Physics* **3**, 92 (2010).
 - [2] A. V. Gorshkov, M. Hermele, V. Gurarie, C. Xu, P. S. Julienne, J. Ye, P. Zoller, E. Demler, M. D. Lukin, and A. M. Rey, *Nat. Phys.* **6**, 289 (2010).
 - [3] M. A. Cazalilla and A. M. Rey, *Reports on Progress in Physics* **77**, 124401 (2014).
 - [4] C. Wu, *Mod. Phys. Lett. B* **20**, 1707 (2006).
 - [5] Z. Cai, H.-H. Hung, L. Wang, and C. Wu, *Phys. Rev. B* **88**, 125108 (2013).
 - [6] N. Blümer and E. V. Gorelik, *Phys. Rev. B* **87**, 085115 (2013).
 - [7] H. Yanatori and A. Koga, *Phys. Rev. B* **94**, 041110 (2016).
 - [8] A. Golubeva, A. Sotnikov, A. Cichy, J. Kuneš, and W. Hofstetter, *Phys. Rev. B* **95**, 125108 (2017).
 - [9] E. Szirmai and M. Lewenstein, *Europhys. Lett.* **93**, 66005 (2011).
 - [10] F. F. Assaad, *Phys. Rev. B* **71**, 075103 (2005).
 - [11] P. Corboz, A. M. Läuchli, K. Penc, M. Troyer, and F. Mila, *Phys. Rev. Lett.* **107**, 215301 (2011).
 - [12] C. Romen and A. M. Läuchli, *Phys. Rev. Research* **2**, 043009 (2020).
 - [13] C. Hofrichter, L. Riegger, F. Scazza, M. Höfer, D. R. Fernandes, I. Bloch, and S. Fölling, *Phys. Rev. X* **6**, 021030 (2016).
 - [14] C. S. Chiu, G. Ji, A. Mazurenko, D. Greif, and M. Greiner, *Phys. Rev. Lett.* **120**, 243201 (2018).
 - [15] R. Yamamoto, J. Kobayashi, T. Kuno, K. Kato, and

- Y. Takahashi, *New J. Phys.* **18**, 023016 (2016).
- [16] M. Miranda, R. Inoue, N. Tambo, and M. Kozuma, *Phys. Rev. A* **96**, 043626 (2017).
- [17] H. Georgi, *Lie Algebras in Particle Physics* (Westview Press, Cambridge, MA, 1999).
- [18] A. Georges, G. Kotliar, W. Krauth, and M. J. Rozenberg, *Rev. Mod. Phys.* **68**, 13 (1996).
- [19] R. W. Helmes, T. A. Costi, and A. Rosch, *Phys. Rev. Lett.* **100**, 056403 (2008).
- [20] M. Snoek, I. Titvinidze, C. Töke, K. Byczuk, and W. Hofstetter, *New J. Phys.* **10**, 093008 (2008).
- [21] A. Sotnikov and W. Hofstetter, *Phys. Rev. A* **89**, 063601 (2014).
- [22] M. Caffarel and W. Krauth, *Phys. Rev. Lett.* **72**, 1545 (1994).
- [23] A. Sotnikov, A. Cichy, and J. Kuneš, *Phys. Rev. B* **97**, 235157 (2018).
- [24] A. Sotnikov, *Phys. Rev. A* **92**, 023633 (2015).
- [25] S. Taie, R. Yamazaki, S. Sugawa, and Y. Takahashi, *Nat. Phys.* **8**, 825 (2012).
- [26] A. Sotnikov, N. Darkwah Oppong, Y. Zambrano, and A. Cichy, *Phys. Rev. Research* **2**, 023188 (2020).
- [27] M. G. Yamada, M. Oshikawa, and G. Jackeli, *Phys. Rev. Lett.* **121**, 097201 (2018).